

1 **Simulating the effect of subsurface drainage on the thermal regime** 2 **and ground ice in blocky terrain, Norway**

3 Cas Renette^{1,2}, Kristoffer Aalstad¹, Juditha Aga¹, Robin Benjamin Zweigel^{1,3}, Bernd Etzelmüller¹,
4 Karianne Staalesen Lilleøren¹, Ketil Isaksen⁴, Sebastian Westermann¹

5

6 ¹Department of Geosciences, University of Oslo, Oslo, Norway

7 ²Department of Earth Sciences, University of Gothenburg, Gothenburg, Sweden

8 ³Centre for Biogeochemistry of the Anthropocene, UiO, Oslo

9 ⁴Norwegian Meteorological Institute, Oslo, Norway

10 *Correspondence to:* Cas Renette (cas.renette@gvc.gu.se)

11 **Abstract.** Ground temperatures in coarse, blocky deposits such as mountain blockfields and rock glaciers have long been
12 observed to be lower in comparison with other (sub)surface material. One of the reasons for this negative temperature anomaly
13 is the lower soil moisture content in blocky terrain, which decreases the duration of the zero curtain in autumn. Here we used
14 the CryoGrid community model to simulate the effect of drainage on the ground thermal regime and ground ice in blocky
15 terrain permafrost at two sites in Norway. The model setup is based on a one-dimensional model domain and features a surface
16 energy balance, heat conduction and advection, as well as a bucket water scheme with adjustable lateral drainage. We used
17 three idealized subsurface stratigraphies, *blocks only*, *blocks with sediment* and *sediment only*, which can be either *drained*
18 (i.e. with strong lateral subsurface drainage), or *undrained* (i.e. without drainage), resulting in six scenarios. The main
19 difference between the three stratigraphies is their ability to retain water against drainage: while the *blocks only* stratigraphy
20 can only hold small amounts of water, much more water is retained within the sediment phase of the two other stratigraphies,
21 which critically modifies the freeze-thaw behaviour. The simulation results show markedly lower ground temperatures in the
22 *blocks only, drained* scenario compared to other scenarios, with a negative thermal anomaly of up to 2.2 °C. For this scenario,
23 the model can in particular simulate the time evolution of ground ice, with build-up during and after snow melt and spring and
24 gradual lowering of the ice table in the course of the summer season. The thermal anomaly increases with larger amounts of
25 snowfall, showing that well drained blocky deposits are less sensitive to insulation by snow than other soils. We simulate
26 stable permafrost conditions at the location of a rock glacier in northern Norway with a mean annual ground surface
27 temperature of 2.0–2.5 °C in the *blocks only, drained* simulations. Finally, transient simulations since 1951 at the rock glacier
28 site (starting with permafrost conditions for all stratigraphies) showed a 100% lowering of the ground ice table in the *blocks*
29 *with sediment, drained* run, 37% lowering in the *sediment only, drained* run and only 2% lowering in the *blocks only, drained*
30 run. The interplay between the subsurface water/ice balance and ground freezing/thawing driven by heat conduction can at
31 least partly explain the occurrence of permafrost in coarse blocky terrain below the elevational limit of permafrost in non-
32 blocky sediments. It is thus important to consider the subsurface water/ice balance in blocky terrain in future efforts on

33 permafrost distribution mapping in mountainous areas. Furthermore, an accurate prediction of the evolution of the ground ice
34 table in a future climate can have implications for slope stability, as well as water resources in arid environments.

35 **1 Introduction**

36 Permafrost is defined as ground that remains at or below 0 °C for two or more consecutive years (Van Everdingen, 1998). It
37 is a common feature in the Arctic and high mountain environments, where permafrost occurs even in mid- and low latitudes
38 (Gorbunov, 1978). Different permafrost zones are classified based on the aerial extent of permafrost presence. These zones
39 are: continuous, discontinuous, sporadic and isolated, where the surface is underlain by permafrost in more than 90%, 50-
40 90%, 10-50% and less than 10% of the land area, respectively (Smith and Riseborough 2002). Snow is an important factor in
41 governing ground temperatures and permafrost distribution within an area (e.g. Zhang et al., 2001; Zhang 2005; Goodrich,
42 1982), especially in mountain areas where permafrost is often associated with a shallow snow cover (e.g. Gissnås et al., 2014;
43 Luetschg et al., 2004). The influence of soil moisture is complicated as it has an impact on the surface energy balance (e.g.
44 Liljedahl et al., 2011), the thermal characteristics of the soil (e.g. Göckede et al., 2017), and freezing/thawing dynamics (e.g.
45 Hinkel et al., 2001; Hinkel and Outcalt, 1994), which can lead to both lower and higher ground temperatures. Finally, the
46 properties of the subsurface material can strongly influence permafrost distribution. In discontinuous mountain permafrost
47 terrain, the lowest-lying permafrost areas are frequently found in coarse, blocky terrain (Harris and Pedersen, 1998). In
48 particular, rock glaciers are frequently found below the general elevation limit of mountain permafrost (Lilleøren and
49 Etzelmüller 2011).

50 In Southern Norway, the lower limit of mountain permafrost is estimated between 1600 m a.s.l. in the west to 1000
51 m a.s.l. in the east (Etzelmüller et al., 2003), while a similar west-east decrease from 800–1000 m a.s.l. to ca. 300 m a.s.l. in
52 the east is observed in Northern Norway (Gissnås et al., 2017). A first Norway-wide inventory of rock glaciers based on aerial
53 imagery was published in 2011 (Lilleøren and Etzelmüller, 2011). The density of rock glaciers is lower than in other mountain
54 permafrost areas which was attributed to a lack of bedrock competence and debris availability as well as to the relative lack of
55 steep topography above the permafrost limit. While this first inventory suggested that active rock glaciers occur only above
56 400 m a.s.l., Lilleøren et al. (2022) recently described rock glaciers near sea level in the area of Hopsfjorden, northern Norway,
57 which feature a limited ice body and are in transition from active to relict. Furthermore, Nesje et al. (2021) presented new
58 evidence for active rock glaciers in southern Norway well below the permafrost limits established in modelling studies
59 (Westermann et al., 2013; Gissnås et al., 2017).

60 Rock glaciers play an important role in the hydrological cycle, especially in arid regions like the Andes, where in
61 some areas more water is stored in rock glaciers than in glaciers (Jones et al., 2019; Azócar and Brenning, 2010). The open
62 debris structure can act as a trap for snow and rock glaciers can store significant quantities of ice or liquid water. Rock glaciers
63 studied in Argentina are an important water resource as they release water mainly during periods of drought (Croce and Milana
64 2002). Sustained ground ice melt as a response to climate warming threatens this water source. Additionally, melting of ground

65 ice can lead to slope instability (e.g. Gruber and Haeberli, 2007; Saemundsson [et al.](#), 2018; Nelson et al., 2001) and damage to
66 infrastructure (e.g. Arenson et al., 2009).

67 The occurrence of a negative temperature anomaly in coarse, blocky deposits has long been recognized (e.g. Liestøl,
68 1966). Harris and Pedersen (1998) found a negative temperature anomaly of 4 to 7 °C in blocky terrain relative to adjacent
69 mineral sediment in mountains in Canada and China. They summarized four hypotheses that explain these anomalies: (a) The
70 Balch effect; (b) chimney effect; (c) continuous air exchange with the atmosphere when no continuous winter snow cover is
71 present; and (d) evaporation of water and sublimation of ice in the summer. The first three of these driving mechanisms relate
72 to air movement in the blocks, while the last hypothesis links characteristics of the water/ice balance to lower ground
73 temperatures in blocky terrain. In the Norwegian mountains, Juliussen and Humlum (2008) showed that blockfields featured
74 a negative temperature anomaly of 1.3 to 2.0 °C. They state that convection in the blockfields is of low importance in creating
75 the anomaly, while the effect was mainly attributed to rocks protruding into and through the snow cover which leads to an
76 increased heat transfer through the snow cover. Gruber and Hoeszle (2008) presented a simple model for the conductive effect
77 of blocks protruding through the snow cover and showed that the mean annual ground temperature is reduced as a result of a
78 lower thermal conductivity of a blocky layer. Additionally, Juliussen and Humlum (2008) argued that a low soil moisture
79 content in permeable blocky debris (due to subsurface drainage in permeable blocky debris) accelerates active layer refreezing
80 in autumn since less latent heat is liberated compared to soils with higher soil moisture content. Cold winter temperatures can
81 therefore penetrate to deeper layers already in early fall/winter, which may lead to decreased overall winter temperatures.
82 However, in spring, the opposite effect is observed when percolating meltwater refreezes at the bottom of the blocky surface
83 layer, leading to rapid ground warming to 0 °C even in deeper layers (e.g. Juliussen and Humlum, 2008; Hanson and Hoeszle,
84 2004; Humlum, 1997).

85 While many of the mechanisms and processes governing the ground thermal regime of blocky terrain are known, a
86 comprehensive quantitative understanding is still lacking. This is particularly relevant for conceptualization in numerical
87 models which generally do not account for the thermal anomaly of blocky terrain. One-dimensional heat flow models have
88 been used in studies to investigate the effect of climate change on permafrost (e.g. Eitzelmüller et al., 2011; Hipp et al., 2012)
89 or to model specific processes in mountain permafrost (e.g. Gruber and Hoeszle, 2008). Since permafrost presence is generally
90 not visible at the surface, numerical models are often used to estimate the permafrost distribution (Harris et al. 2009). However,
91 as most models neither include a transient representation of the subsurface water and ground ice balance (e.g. Westermann et
92 al., 2013) nor reproduce the thermal anomaly in blockfields (e.g. Obu et al., 2019), the resulting permafrost maps likely show
93 biased ground temperatures and permafrost extent in mountain areas.

94 The CryoGrid community model (Westermann et al., 2022) is a simulation toolbox that can calculate ground
95 temperatures and water/ice contents in permafrost environments. It largely builds on the well-established CryoGrid 3 model
96 (Westermann et al. 2016) which has been used in e.g. peat plateaus and palsas (Martin et al. 2021), ice-wedge polygons
97 (Nitzbon et al. 2019) and boreal forests (Stuenzi et al. 2021) and has a broad range of applications, including the representation

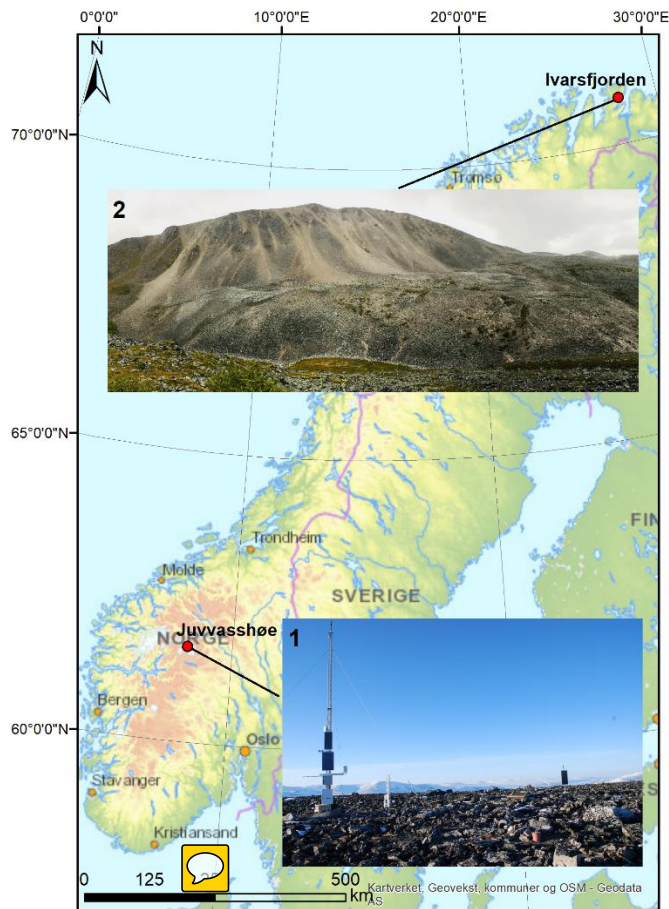
98 of lateral drainage regimes (Martin et al., 2019), representation of steep rock walls (Schmidt et al., 2021) and massive ice
99 bodies. In the following, the CryoGrid community model is referred to as “CryoGrid” for simplicity.

100 In this study, we present CryoGrid simulations of the coupled heat and water/ice balance for blocky terrain in Norway
101 and evaluate the impact of the ground stratigraphy and the drainage regime on ground temperatures. The model is set up with
102 forcing data for two Norwegian permafrost sites, namely a blockfield site in the high mountains in southern Norway and a
103 rock glacier site near sea level in northern Norway. The employed model scheme does not account for air movement and rocks
104 protruding the snow cover as the “classic” causes for the negative thermal anomaly of blocky terrain, but is capable of
105 simulating the seasonal dynamics of the ground ice table in blocky terrain. The goal of the study is to evaluate to what extent
106 the thermal anomaly in blocky terrain can be simulated by such a comparatively simple scheme which could in principle be
107 integrated in larger-scale permafrost modelling and mapping efforts. In particular, we investigate the interplay with the
108 seasonal snow cover and discuss the impact on the permafrost distribution in mountain environments.

109 2 Study sites

110 2.1 Juvvasshøe, southern Norway

111 Juvvasshøe (61°40 N, 08°22 E, 1894 **m.a.s.l.**) (Fig. 1) is a site located in Jotunheimen in the southern Norwegian mountains,
112 well above the tree line. A 129 m deep borehole was drilled in August 1999 in the PACE (Permafrost and Climate in Europe)
113 project (Harris et al., 2001). Continuous data streams from this PACE borehole are available with the exception of a gap
114 between 21 December 2011 to 24 April 2014. The site is located in an extensive block field on a mountain plateau with sparse
115 vegetation cover. The bedrock (crystalline rocks, Farbrot et al., 2011) is located at approximately 5 m depth, the first meter
116 consists of large stones and boulders and the ground below mainly consists of cobbles (Isaksen et al., 2003). Between 2000
117 and 2004, Isaksen et al. (2007) measured a mean annual air temperature (MAAT) at 2 m height of -3.3 °C. The mean ground
118 temperature (~~MGT~~) at 2.5 m below the surface during this period was -2.5 °C. The mean annual precipitation was estimated
119 to be between 800 and 1000 mm. The site is extremely wind-exposed, resulting in a low snow thickness due to wind drift.
120 Hipp et al. (2012) described a snow depth of less than 20 cm, while the snow thickness in surrounding, lower-lying and less
121 exposed sites can be up to 140 cm. Isaksen et al. (2007) measured the difference between the mean annual ground surface
122 temperature (~~MAGST~~) and ~~mean annual air temperature (MAAT)~~, which is the surface offset, at exposed and less exposed
123 sites in this area. At sites with a significant snow cover, the surface offset was more than 2 °C, while at exposed (including
124 Juvvasshøe) sites this offset is generally below 1 °C. The permafrost thickness at the PACE borehole was estimated to be
125 approximately 380 m (Isaksen et al., 2001), with the lower permafrost limited at ca. 1450 m.a.s.l. (Farbrot et al., 2011). The
126 thickness of the active layer increased from 215 cm in 1999 (Isaksen et al., 2001) to ca. 250 cm in 2019 (Etzelmüller et al.,
127 2020). A weak zero curtain effect suggests a low water content in the active layer (Isaksen et al., 2007). A warming of 0.2 °C
128 per decade and 0.7 °C per decade in surface air temperature and ground surface temperature, respectively, occurred between
129 2000 and 2019 (Etzelmüller et al., 2020).



130

131 **Figure 1: Location of the two sites in Norway (© Norwegian Mapping Authority). (1) blockfield at Juvasshøe (1894 m.a.s.l.), (2)**
 132 **rock glacier at Ivarsfjorden (60–160 m.a.s.l.).**

133 2.2 Ivarsfjorden rock glacier, northern Norway

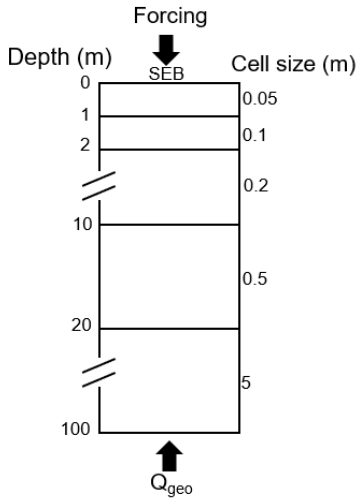
134 Ivarsfjorden is a small fjord arm of the larger Hopsfjorden, located on the Nordkinn peninsula in the Troms and Finnmark
 135 county in northern Norway (Fig. 1). Deglaciated around 14–15 kyr BP (Romundset et al., 2011), the peninsula is dominated
 136 by flat mountain plateaus of exposed bedrock, *in situ* weathered material and coarse grained till (Lilleøren et al., 2022), which
 137 feature steep slopes towards the sea. The coastal areas of Finnmark have a wet maritime climate, with mean annual precipitation
 138 around 1000 mm (Saloranta, 2012). Lilleøren et al. (2022) describe a MAAT of 1.6 °C between 2010 and 2019 in the area of
 139 the rock glacier, which lies in a southwest-northeast trending valley at an elevation extent of roughly 60 to 160 m a.s.l.. The
 140 mountain at its east (443 m.a.s.l.) serves as the source area with rockfall debris and coarse talus slopes being common. The
 141 bedrock in Ivarsfjorden consists of sandstones and phyllites (NGU, 2008). Sandstones often generate coarse, bouldery material,
 142 which is favorable for the formation of rock glaciers (Haeberli et al. 2006). The rock glacier in Ivarsfjorden is northwest facing
 143 and has previously been interpreted as relict (Lilleøren and Etzelmüller, 2011), but a detailed analysis showed that a limited

144 ice core might still be present (Lilleøren et al., 2022). A negative MAAT around 100 to 150 years ago is an indication that
145 rock glaciers in this area were likely active at the end of the Little Ice Age (LIA). Refraction Seismic Tomography ~~(RST)~~
146 surveys indicate a porous air-filled stratigraphy such as blocky talus deposits at the near-surface at parts of the rock glacier.
147 While observed **MAGSTs** between 2015 and 2020 are all positive, negative surface temperatures during summer have been
148 observed by a thermal camera at the front slope of the rock glacier. This is likely an indication of the chimney effect and thus
149 of connected voids that support air flow.

150 **3. Methods**

151 **3.1 The CryoGrid community model**

152 CryoGrid is a simulation toolbox for ground thermal simulations that can be applied to a wide range of modelling tasks in the
153 terrestrial cryosphere thanks to its modular structure (see Westermann et al., 2022 for details). It is mainly applied in permafrost
154 environments, using the finite difference method to transiently simulate ground temperatures. We use a one-dimensional model
155 column with a domain depth of 100 m (as ~~in~~-e.g. Westermann et al., 2016; Schmidt et al., 2021) and grid cell sizes increasing
156 with depth (Fig. 2). The lower boundary condition is provided by a constant geothermal heat flux. The upper boundary results
157 from solving the surface energy balance, including both radiative and turbulent heat fluxes, as well as the heat flux in the
158 ground. In order to compute the surface energy balance, atmospheric forcing data are required (Sect. 3.2). To calculate ground
159 temperatures, both conductive heat transfer following Fourier's law and advection of heat with vertically moving water is
160 taken into account (Westermann et al., 2022). The freezing characteristic of subsurface water/ice depends on the soil type,
161 either following Painter and Karra (2014) for sediments, or set to free water (water changes state at 0 °C, Westermann et al.,
162 2022) for subsurface material with large pores/voids, such as blocky terrain. To define the properties of the subsurface material,
163 a stratigraphy of volumetric mineral, organic, water and ice contents and the field capacity (the ability to hold water against
164 gravity) must be provided (Westermann et al., 2022).



165

166 **Figure 2: Schematic of the model grid, indicating cell sizes at different depths and upper and lower boundary conditions. As upper**
 167 **boundary condition, the surface energy balance (SEB) forced by near-surface meteorological data is used. The lower boundary**
 168 **condition is provided by a constant geothermal heat flux.**

169 For soil hydrology, a gravity driven bucket scheme is used (Westermann et al 2022). Rainfall provided by the model
 170 forcing is added to the uppermost grid cell, while evaporation is determined by the surface energy balance calculations (note
 171 that we consider unvegetated surfaces and thus do not account for transpiration). Water that is in excess of the field capacity
 172 infiltrates downwards until either the water table or a non-permeable layer, such as a frozen grid cell is reached. If all grid cells
 173 are saturated, excess water is removed as surface runoff. We use a one-dimensional model setup, but simulate lateral drainage
 174 of water by introducing a seepage face, i.e. a lateral boundary condition for water fluxes representing flow between the
 175 saturated grid cells of the model domain and a stream channel (or the atmosphere) to which the water can freely flow out from
 176 the subsurface (e.g. Scudeler et al. 2017). Using the elevation of the water table, z_{wt} (computed as the elevation of the
 177 uppermost saturated grid cell), lateral water fluxes F_i^{lat} are derived for all saturated unfrozen grid cells i below the water table
 178 (i.e. at elevations $z_i < z_{wt}$) as

$$179 \quad F_i^{lat} = -K_H \frac{z_{wt} - z_i}{d^{lat}}, \quad (1)$$

180 where K_H is the saturated hydraulic conductivity, d^{lat} is the lateral distance to the seepage face and the flux is determined by
 181 the difference between the hydrostatic potential (proportional to z_{wt}) of the water column and the gravitational potential of
 182 free water at the elevation of each cell (proportional to z_i). Note that Eq. (1) is an approximation for small changes of the water
 183 table and small outflow fluxes for which the potential in the saturated zone can be approximated by the hydrostatic potential.
 184 The parameter d^{lat} is used to control the strength of the drainage, with small distances resulting in a well-drained column,
 185 while high values lead to suppressed drainage. In this study, we consider the two confining cases with a small and large value
 186 of d^{lat} , respectively (Sect. 3.3). In the former, water from rain or ground ice melt is removed rapidly, effectively preventing

187 the soil water from pooling up, while drainage is negligible in the former, so that the setup corresponds to a classic one-
188 dimensional model scheme.

189 The snow model used in this study was introduced by Zweigel et al. (2021) and is based on the Crocus snow scheme
190 (Vionnet et al. 2012) which accounts for snow microphysics and is designed to reproduce a realistic snow pack structure (see
191 Vionnet et al. 2012 for defining equations; Zweigel et al. 2021 for implementation in CryoGrid). Snowfall is added with density
192 and microphysical properties derived from model forcing data, in particular air temperature and wind speed. The snow density
193 evolves due to compaction by the overburden pressure of overlying snow layers, as well as wind compaction and refreezing
194 of melt- and rainwater (Vionnet et al. 2012). The amount of snowfall from the forcing data can be adjusted by a so-called
195 *snowfall factor*, sf , with which the snowfall rate from the model forcing is multiplied. With this, the effects of wind-induced
196 snow redistribution on ground temperatures can be represented at least phenomenologically (Martin et al., 2019), using $sf < 1$
197 for areas with net snow ablation and $sf > 1$ for areas with net deposition.

198 3.2 Downscaling of model forcing

199 The meteorological data used to force the CryoGrid model were generated by applying TopoSCALE, a topography-based
200 downscaling routine (Fiddes and Gruber, 2014), to ERA5 reanalysis data (Hersbach et al., 2020). TopoSCALE is employed in
201 cryosphere applications in complex terrain, including estimating mountain permafrost distribution (Fiddes et al., 2015), snow
202 data assimilation (Aalstad et al., 2018; Fiddes et al., 2019), and downscaling regional climate model output (Fiddes et al.,
203 2022). ERA5 output is provided as interpolated point values on a regular latitude-longitude grid at a resolution of 0.25° at an
204 hourly frequency, both at the surface level, corresponding to Earth's surface as represented in the reanalysis, and at 37 pressure
205 levels in the atmosphere from 1000 to 1 hPa. We considered data for the reanalysis period from 1951 to 2019 at three-hourly
206 resolution. As input to TopoSCALE, we obtained from the surface level: 2 ~~meter~~ air and dewpoint temperature, 10 ~~meter~~
207 meridional (northward) and zonal (eastward) wind velocity components, surface pressure, constant surface geopotential,
208 incoming longwave radiation, incoming shortwave radiation, and total precipitation. From the pressure levels we acquired: air
209 temperature, specific humidity, zonal and meridional wind velocity components, and dynamic geopotential. For Juvvasshøe at
210 ~~1894 m a.s.l.~~ we used all levels in the range 900 hPa to 700 hPa, while for the lower elevation Ivarsfjorden rock glacier at ~~60-~~
211 ~~160 m a.s.l.~~ we used all levels between 900 hPa and 1000 hPa. To account for terrain shading in the downscaling routine, a
212 digital elevation model (DEM) is required, for which we use the mosaic version of the ArcticDEM with a resolution of 32 m
213 (Porter et al., 2018) at both sites. TopoSCALE delivers all meteorological forcing data required to run CryoGrid: near surface
214 air temperature, specific humidity, wind speed, incoming longwave radiation, incoming shortwave radiation, as well as
215 snowfall and rainfall.

216 3.3 Model setup

217 Three idealized ground stratigraphies are set up in order to investigate the effect of water drainage on the ground thermal
218 regime and ground ice dynamics in blocky terrain. These are referred to as the *blocks only*, *blocks with sediment* and *sediment*

219 *only* stratigraphies (Table 1) in the following. The *blocks only* stratigraphy consists of a coarse block layer with 50% porosity
 220 and air-filled voids which is assigned low field capacity of 1% (Table 1), i.e. the surfaces of the coarse blocks retain only little
 221 water. This idealized stratigraphy is designed to represent an active rock glacier where finer sediments resulting from
 222 weathering and erosion processes are transported towards the tongue of the rock glacier. Furthermore, Dahl (1966) observed
 223 that blockfields on slopes more often do not contain a fine sediment fraction between the blocks in northern Norway, so that
 224 the *blocks only* stratigraphy can also represent active blockfields. The second stratigraphy, *blocks with sediment*, is designed
 225 to represent blocky terrain where the voids are filled by finer sediments. This is often observed in blockfields on more flat
 226 surfaces, which are more likely to retain finer sediment within their pores (as in Isaksen et al., 2003 and Dahl 1966). We again
 227 consider coarse blocks with 50% porosity (as for the *blocks only* stratigraphy), but as the voids are filled with fine sediments
 228 (which again are assumed to have 50% porosity), the overall porosity is only 25%. Furthermore, a significantly higher field
 229 capacity than for the *blocks only* stratigraphy is assigned as more water can be held in the finer pores of the sediment fraction.
 230 Finally, the *sediment only* stratigraphy serves as a control scenario for a soil without blocks. It contains sediment with 50%
 231 porosity and a high field capacity due to the water holding capacity of the fine-grained sediment material. For all stratigraphies,
 232 bedrock (3% porosity and saturated conditions, e.g. Hipp et al. 2012; Fabrot et al. 2011) is assumed below 5 m depth, which
 233 is in line with observations from Isaksen et al. (2003) at Juvvasshøe. Finally, none of the stratigraphies contain soil organic
 234 matter. We emphasize that the stratigraphies are in qualitative agreement with field observations of air and sediment-filled
 235 block layers in Norway, but the assumed porosities of 50% for both the block layer and the sediments represent idealized
 236 scenarios. However, we perform a sensitivity analysis for different porosity values (see **Supplement**) to investigate the impact
 237 of this parameter on the simulation results.

238

239 **Table 1: Mineral content, porosity, field capacity (all in vol. fraction) and soil freezing characteristic for the three idealized**
 240 **subsurface stratigraphies.**

Name	mineral	porosity	field capacity	soil freezing characteristic
<i>Blocks only</i>	0.5	0.5	0.01	Free water
<i>Blocks with sediment</i>	0.75	0.25	0.15	Free water
<i>Sediment only</i>	0.5	0.5	0.25	Sand

241

242 For the geothermal heat flux lower boundary condition, a value of 0.05 Wm^{-2} is used, which is a typical value for Norway used
 243 in previous modelling studies (Westermann et al., 2013).

244 To investigate the effect of subsurface drainage on ground temperatures and ground ice conditions, we distinguish *undrained*
 245 and *drained* scenarios by using two different values of d^{lat} (Eq. 1) for in the idealized stratigraphies. **A d^{lat} value of 10^4 m is**
 246 **used for *undrained* cases,** which emulates conditions at a flat surface, resulting in a to a good approximation one-dimensional

247 water balance, where only surface water is removed. For the *drained* cases, a d^{lat} value of 1 m is used, which results in well-
 248 drained conditions which are typical in sloping terrain. For the saturated hydraulic conductivity K_H , a fixed value of 10^{-5} m s^{-1}
 249 ¹ is used for all stratigraphies, although the true hydraulic conductivities almost certainly differ between stratigraphies.
 250 However, the key parameter controlling lateral water fluxes in Eq. 1 is in reality the “drainage timescale” K_H/d^{lat} [s^{-1}], which
 251 is varied by four orders of magnitude between $K_H/d^{lat} = 10^{-5} \text{ s}^{-1}$ ($d^{lat} = 1 \text{ m}$, well-drained conditions) and $K_H/d^{lat} = 10^{-9} \text{ s}^{-1}$
 252 ($d^{lat} = 10^4 \text{ m}$ undrained conditions). As the study setup is designed to analyze these two “confining cases”, it is sufficient to
 253 only vary d^{lat} and leave K_H constant for simplicity. Further sensitivity tests for d^{lat} and K_H are provided in the
 254 Supplement. With the exception of the *snowfall factor* (see Sect. 3.3.1 to 3.3.3), the parameters in the snow model are kept
 255 constant in all model runs, using a surface emissivity of 0.99, a roughness length of 10^{-3} m , a saturated hydraulic conductivity
 256 of 10^{-4} m s^{-1} and a field capacity of 0.05 (Westermann et al. 2022). For the ground surface, we used an albedo of 0.15, emissivity
 257 of 0.99, and a roughness length of 10^{-3} m .

258 We perform three types of model simulations which differ in their overall purpose. For *validation* runs (Sect. 3.3.1),
 259 we adjust subsurface stratigraphy and *snowfall factor* in order to compare model results with the available field measurements
 260 from the two study sites. *Equilibrium* runs (Sect. 3.3.2) and *transient* runs (Sect. 3.3.3) are designed to explore the sensitivity
 261 of the simulated ground thermal regime towards the three idealized stratigraphies (Table 1) and the two drainage cases. An
 262 overview of the basic settings of the different simulation types is provided in Table 2.

263

264 **Table 2: Overview of basic model settings for the different simulation types. A spin-up of subsurface temperatures is achieved by**
 265 **repeated simulations for the spin-up period (until a stable temperature profile is reached), before the actual model run for the**
 266 **simulation period is conducted. “Idealized” stratigraphy and drainage refers to three subsurface stratigraphies (Table 1) combined**
 267 **with two types of drainage conditions. See Sect. 3.3.1 to Sect. 3.3.3 for details.**

Simulation type	Site	Spin up period	Simulation period	Stratigraphy and drainage	Snowfall factor
<i>Validation</i>	Juvvasshøe	1951-2010	2010-2019	Best-fit	0.25
	Ivarsfjorden	1951-2016	2016-2019	Best-fit	1
<i>Equilibrium</i>	Juvvasshøe	2000-2010	2000-2010	Idealized	0.0, 0.25, 0.5, 0.75, 1.0, 1.5
	Ivarsfjorden	1962-1971	1962-1971	Idealized	0.0, 0.25, 0.5, 0.75, 1.0, 1.5
<i>Transient</i>	Juvvasshøe	1962-1971	1951-2019	Idealized	0.25
	Ivarsfjorden	1962-1971	1951-2019	Idealized	1

268

269 3.3.1 Validation runs

270 As a prerequisite for conducting model experiments on ground stratigraphy and drainage (Sects. 3.3.2, 3.3.3), validation runs
271 are set up to show that the model can reproduce key characteristics of the thermal regime at the two sites in a satisfactory
272 manner (based on available observations). Furthermore, we use the observations to determine the best-fitting *snowfall factor*
273 for the two sites which is subsequently used in the transient runs (Sect. 3.3.3). At Juvvasshøe, temperature measurements in a
274 borehole are available from 2000 to 2019, allowing a comparison at different depths. At the Ivarsfjorden rock glacier site,
275 observations of ground temperature at deeper depths are lacking, but measurements of near-surface ground temperatures are
276 available from July 2016 to July 2019 (Lilleøren et al., 2022). These are compared to simulation results to ensure that the
277 model reproduces the observed surface offset between air and ground surface, largely caused by the winter snow cover (e.g.
278 Martin et al., 2019; Schmidt et al., 2021). At both sites, the model is ran for the entire period of available forcing data, leaving
279 at least 60 years for the model spin-up which is sufficient to analyze ground temperatures in uppermost meters of the ground
280 column.

281 Manual adjustment of the ground stratigraphy (porosity and thus mineral content) and snowfall factor are performed
282 until a good fit with daily measurements is achieved. At Juvvasshøe, based on observations of blocks and smaller cobbles with
283 finer sediments down to the onset of bedrock at a depth of 5 m (Isaksen et al. 2003), the *blocks with sediment* stratigraphy is
284 used as a starting point to vary porosities until a good fit is achieved. As this site is extremely exposed to wind and most snow
285 is blown away (Isaksen et al. 2003; Westermann et al., 2013), the snowfall factor is stepwise decreased to values below one to
286 improve the model performance. At Ivarsfjorden, we considered 11 temperature loggers within the rock glacier outline (Fig.
287 1d in Lilleøren et al., 2022), of which all except for one are placed on the relict surface of the rock glacier (Fig. 2a in Lilleøren
288 et al., 2022). On the relict surface, deposition of finer sediment in between blocks is more likely than on the active surface,
289 due to the lack of movement. Here, the *blocks with sediment* stratigraphy is considered appropriate and used as starting point
290 for the calibration. At both sites, the root-mean-square-error (RMSE) and bias are calculated in order to provide an objective
291 measure of the model fit. At Juvvasshøe this was accomplished for daily values at 0.4 m and 2 m depth, while at Ivarsfjorden
292 the mean daily ground surface temperature of the loggers within the rock glacier outline is used.

293 3.3.2 Equilibrium runs

294 The goal of equilibrium runs is to investigate the sensitivity of the ground thermal regime towards ground properties and
295 drainage conditions, using both the *undrained* and *drained* setup for the three idealized stratigraphies (Table 1) which results
296 in six scenarios. As the heavily wind-affected snow cover is a key source of spatial variability in ground temperatures in the
297 Norwegian mountains (Gisnås et al., 2014; Gisnås et al., 2016), the model is run for a range of snowfall factors between 0.0
298 and 1.5 (Table 2) for each scenario. This analysis allows us to identify the magnitude of the thermal anomaly that the subsurface
299 drainage induces at various amounts of snow, as well as estimate the threshold snow amount for permafrost existence in the
300 six scenarios. This analysis is performed for equilibrium conditions for 10 year periods of roughly stable climate, which is

301 iterated three times until a steady state temperature profile of the uppermost 5 meters is established. For Juvvasshøe, the period
302 2000 to 2010 is selected as the model can be initialized with real-time borehole data. For Ivarsfjorden, the comparatively cold
303 period 1962 to 1971 is selected as this relatively stable period is the coldest period in the available forcing data and thus the
304 closest to Little Ice Age climate conditions, when the Ivarsfjorden rock glacier was very likely active (Lilleøren et al., 2022).

305 **3.3.3 Transient runs**

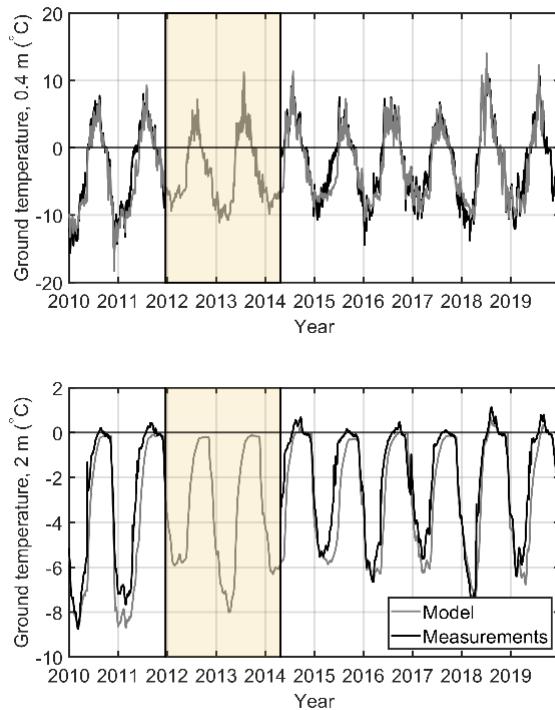
306 The goal of the transient runs is to analyze the effect of ground stratigraphies and drainage conditions on the transient response
307 of ground temperatures and ice tables to climate warming. For this purpose, we perform model simulations from 1951 to 2019,
308 when air temperatures have increased by more than $1\text{ }^{\circ}\text{C}$ in Norway. To initialize simulations, we perform a model spin-up by
309 iterating three times over the coldest 10 year period in the forcing data (1962 – 1971) which is sufficient to achieve a stable
310 ice table. This is the same period as in the equilibrium runs (see Sect. 4), for which it was selected to capture permafrost
311 conditions at the Ivarsfjorden rock glacier site (see Sect. 4). Thus, the transient runs allow us to analyze the evolution of the
312 permafrost towards the warming of the recent decades. We only use the best fitting snowfall factor (Table 2), as derived from
313 the validation runs (Sect. 3.3.1), but again perform simulations for the three idealized stratigraphies and *undrained* and *drained*
314 conditions. This way, we can evaluate whether different ground stratigraphies or drainage conditions lead to different warming
315 rates of ground temperatures, as well as different thresholds for permafrost thaw.

316 **4. Results**

317 **4.1 Comparison to in-situ measurements**

318 The results of the *validation runs* at Juvvasshøe are compared with measured daily ground temperatures at the PACE borehole
319 (Etzelmüller et al, 2020). Figure 3 shows the comparison of measured ground temperatures with modelled temperatures at 0.4
320 and 2.0 m depth for the best fitting model configuration. The snowfall factor for this model setup is 0.25, i.e. incoming snowfall
321 is reduced by 75% in order to capture the effect of snow ablation due to wind drift. This resulted in mean annual maximum
322 snow depths of 34 cm, in broad agreement with observations from the site (Iskasen et al., 2003) and earlier modeling studies
323 at the site (Westermann et al., 2013). The subsurface stratigraphy for this model configuration is highly similar to the *blocks*
324 *with sediment* stratigraphy, but with a slightly lower porosity of 0.2 (i.e. a volumetric mineral content of 0.8). This would for
325 example correspond to blocks and cobbles with a porosity of 0.4 (0.5 for *blocks with sediment*), filled with fine sediments with
326 a porosity of 0.5 (and field capacity 0.25), which is plausible given the broad characteristics of the observed borehole
327 stratigraphy (Isaksen et al., 2003). This configuration used *drained* conditions, although differences with *undrained* conditions
328 are minimal for this stratigraphy. For daily temperatures at 0.4 m depth, the RMSE and bias are $2.1\text{ }^{\circ}\text{C}$ and $-0.6\text{ }^{\circ}\text{C}$, respectively,
329 while they are $1.2\text{ }^{\circ}\text{C}$ and $-0.7\text{ }^{\circ}\text{C}$ at 2 m depth. There is a mismatch in the timing of spring temperatures at 2 m depth in several
330 years, for which modelled temperatures increase later than measured values. This is likely a result of differences in the snow
331 melt, as the snowpack dynamics resulting from wind redistribution is not completely captured by the snowfall scaling with a

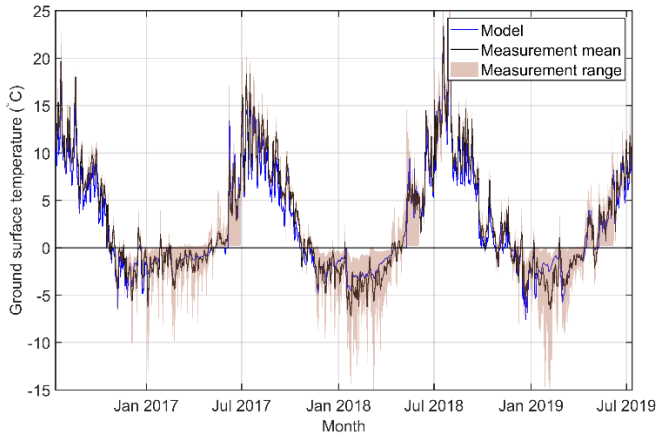
332 constant snowfall factor (e.g. Martin et al., 2019). Furthermore, the uppermost 1 m contain large stones and boulders, while
333 the layer below is characterized by smaller stones and cobbles (Isaksen et al. 2003), so that a ground stratigraphy with two
334 layers in the uppermost 5 m may further improve the performance of the simulations.



335

336 **Figure 3: Modelled and measured ground temperature at the PACE borehole in Juvvasshøe at 0.4 m (upper) and 2.0 m (lower)**
337 **depth. The shaded area indicates a period when no borehole data are available.**

338 At the rock glacier in Ivarsfjorden, a comparison between modelled and measured temperature is performed for
339 average daily ground surface temperatures, using the mean of the measurements at 11 sites within the rock glacier as target for
340 the comparison (Fig. 4). The best-fitting model configuration was found to be the *blocks with sediment* stratigraphy and a
341 snowfall factor of 1.0, resulting in an RMSE of 1.3 °C and a bias of -0.4 °C. As in Juvvasshøe, the configuration used *drained*
342 conditions, while differences with *undrained* conditions are small. Fig. 4 also shows the significant spatial variability of ground
343 surface temperatures, which is particularly large in winter. Also in periods, when the simulation results and the mean of the
344 measurements visibly deviate, the simulations remain within the range of the measurements. While there are some deviations
345 between the observations and simulation results at both Juvvasshøe and Ivarsfjorden, we conclude that the model setup,
346 including the model forcing, can capture the general ground surface temperature regime at both sites which is a prerequisite
347 for obtaining meaningful results from the *equilibrium* and *transient runs*.

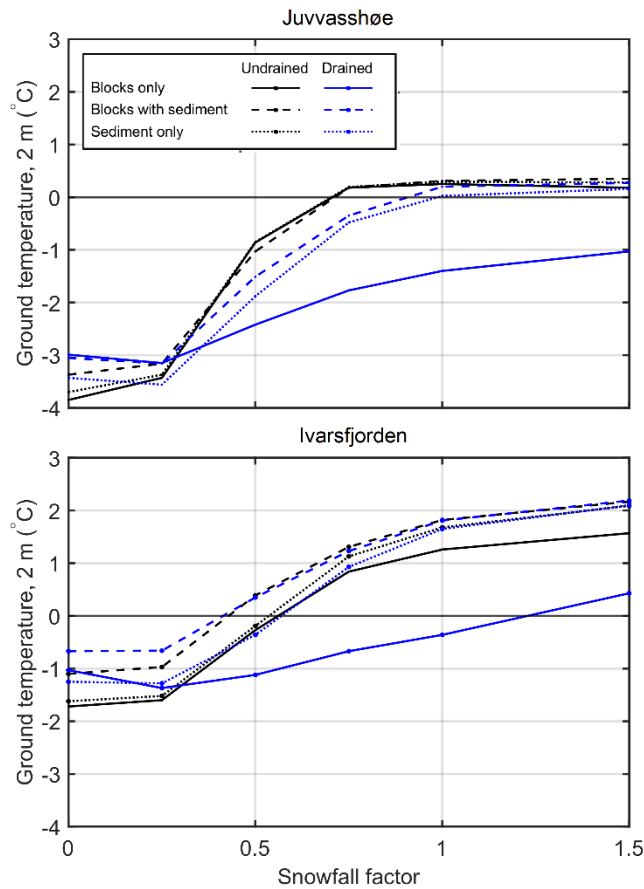


348

349 **Figure 4: Daily modelled and measured ground surface temperatures in Ivarsfjorden from July 2016 to July 2019. The shaded area**
 350 **indicates the minimum to maximum range of measured daily values from 11 loggers (based on Lilleøren et al., 2022), while the black**
 351 **line represents the mean value of all loggers.**

352 4.2 Equilibrium ground temperatures and sensitivity to snow

353 **Fig. 4** shows the average ground temperature at 2 m depth for the three stratigraphies, the *drained* and the *undrained* scenario,
 354 and different snowfall factors at both sites. At both sites there is a clear pattern of lower temperatures in the *blocks only*,
 355 *drained* scenario (solid blue line) compared to all five other scenarios. For snowfall factors of 0.75 and larger, the difference
 356 in ground temperature between *blocks only, drained* and the other scenarios is in the range of 1.1 °C and 1.8 °C at Juvvasshøe
 357 and in the range of 1.1 °C and 2.2 °C at Ivarsfjorden. This shows that the magnitude of the negative thermal anomaly increases
 358 with a larger amount of snowfall. Results of the sensitivity study to porosity of the soil (see Supplement) show that mean
 359 ground temperatures are within 0.4 °C between the highest and lowest porosity tested.



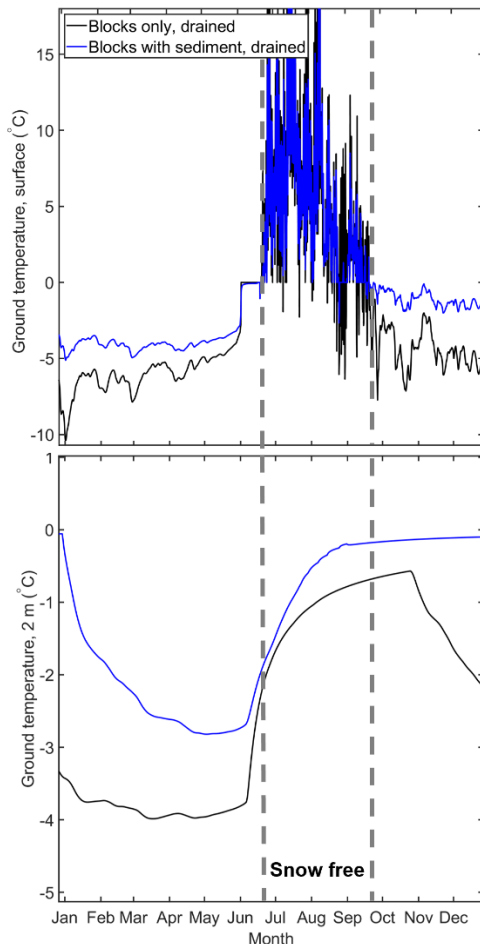
360

361 **Figure 5: Equilibrium ground temperature at 2 m depth for three idealized stratigraphies (Table 1) and different snowfall factors.**
 362 **Each data point represents one model run of one of the six scenarios at a certain snowfall factor.**

363 Annual maximum snow depths at a snowfall factor of 1.0 are between 1.5 m and 2.4 m at Juvvasshøe and between
 364 0.4 m and 1.0 m at Ivarsfjorden. At Juvvasshøe, all three *undrained* scenarios feature positive ground temperatures at snowfall
 365 factors of 0.75 and above, which corresponds to permafrost-free conditions. Temperatures in the *blocks with sediment, drained*
 366 and *sediment only, drained* runs are positive for a snowfall factor of 1.0 and above. The ground temperature in the *blocks only,*
 367 *drained* runs remains below -1.0 °C for all snowfall scenarios. A similar pattern is seen in Ivarsfjorden, although a snowfall
 368 factor of 1.5 results in positive temperatures for the scenario *blocks only, drained* which is clear evidence of the overall warmer
 369 ground temperatures. Temperatures for the *blocks with sediment* stratigraphy are positive for snowfall factors exceeding 0.5,
 370 and exceeding 0.75 for the other scenarios (with the exception of the *blocks only, drained* scenario, see above). For snowfall
 371 factors above 0.25, ground temperature at 2 m depth increase with snow depth as a result of increased insulation of the ground
 372 during winter. However, the increase from a snowfall factor of 0 to 0.25 leads to a slight cooling for the *drained* scenarios as
 373 opposed to a slight warming in the *undrained* scenarios. The reason for this cooling is likely the higher winter albedo of the

374 completely snow-free ground (for snowfall factor zero), which outweighs the insulating of the shallow snow cover for snowfall
375 factor 0.25.

376 **Fig. 5** shows simulated temperatures for one year at the ground surface and 2 m depth for drained conditions for both
377 *blocks only* and the *blocks with sediment* scenarios for Juvvasshøe (snowfall factor 0.75). While ground surface temperatures
378 are largely similar during the snow-free summer season, they decrease much faster in fall for the *blocks only* compared to the
379 *blocks with sediment* scenario, for which the slow refreezing of the active layer leads to a prolonged warming of the ground
380 surface from below. In the *blocks only* scenario, on the other hand, the active layer contains only little water, so that refreezing
381 occurs within only a short time period. The rapid cooling in the *blocks only* scenario is also visible within the permafrost table
382 at 2 m depth, resulting in lower winter temperatures compared to the *blocks with sediment* curve and thus explaining the
383 simulated differences in **MAGT**.

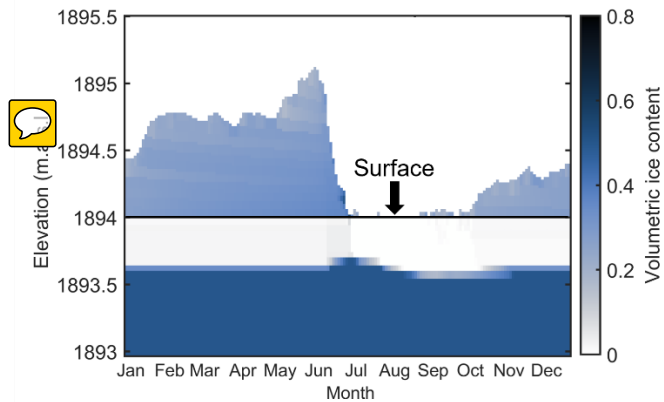


384

385 **Figure 6: Modelled ground temperature at 0.05 m (top) and 2 m (bottom) depth for the *blocks only, drained* and *blocks with sediment,***
386 ***drained* scenarios during a year of an equilibrium run at Juvvasshøe for $sf = 0.75$. The snow-free summer season is highlighted. Note**
387 **that the upper plot is truncated at 17 °C, maximum summer temperatures are 26 °C in both scenarios.**

388

389 **Fig. 6** shows the corresponding snow cover and volumetric ground ice content in the upper meter of the ground for
390 the *blocks only, drained* scenario. A largely stable ground ice table forms already at a depth of about 0.5 m, while the active
391 layer is almost free of ground ice in winter, corresponding to the low water contents for thawed condition, enabling rapid
392 refreezing and thus strong cooling during winter. During and after snow melt, meltwater infiltrates in the blocky layer and
393 refreezes at the then very cold ice table, resulting in the formation of new ground ice which slowly melts during the course of
394 summer. The slight increase of the ground ice table in early winter is due to refreezing of residual water above the ice table
395 from rain and snow melt events in October which has not fully drained before refreezing.



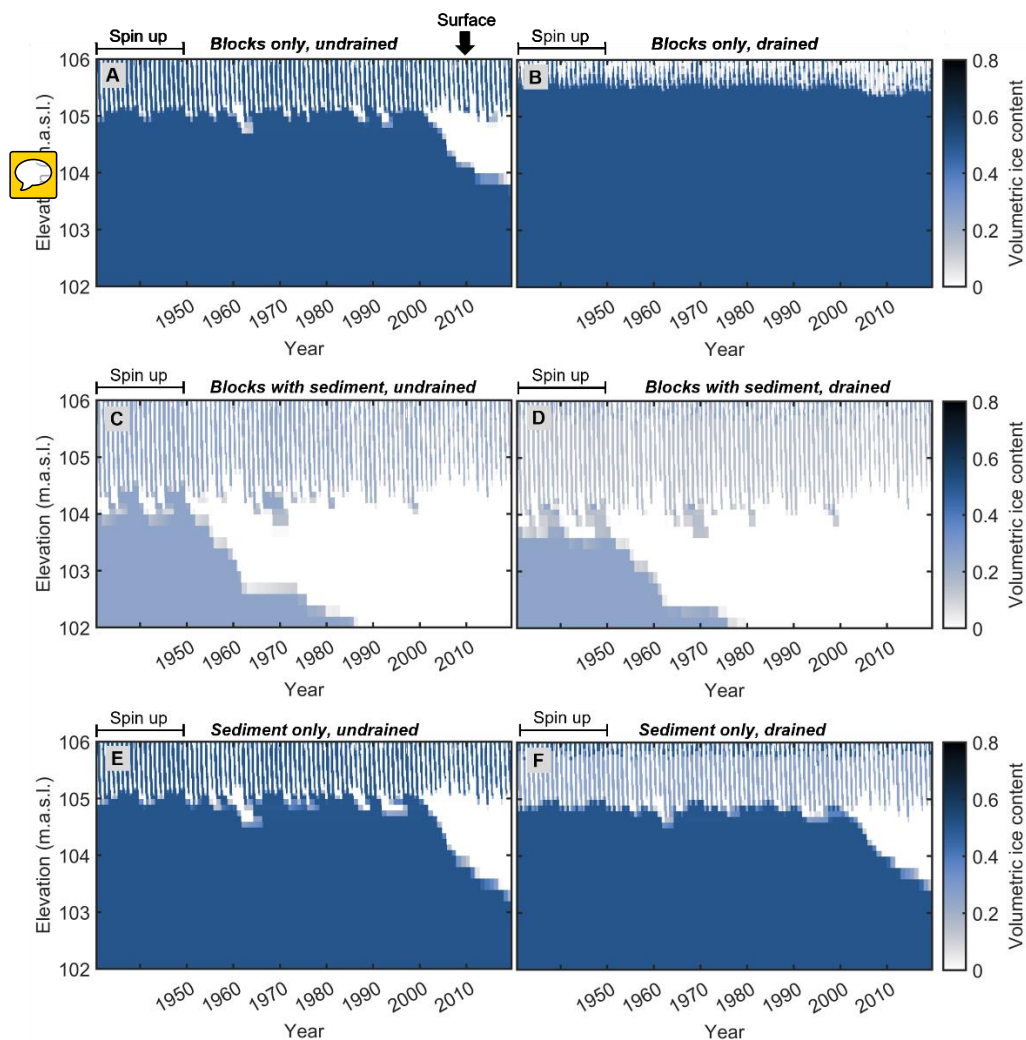
396

397 **Figure 7: Modelled volumetric ground ice content in the upper 1 m of the ground (below 1894 m) and the snow cover (above 1894**
398 **m) for the *blocks only, drained* scenario, during one year of an equilibrium run at Juvvasshøe for $sf = 0.75$. Note the rise of the ground**
399 **ice table in June after infiltrated snow melt water refreezes.**

400 4.3 Transient response to climate warming

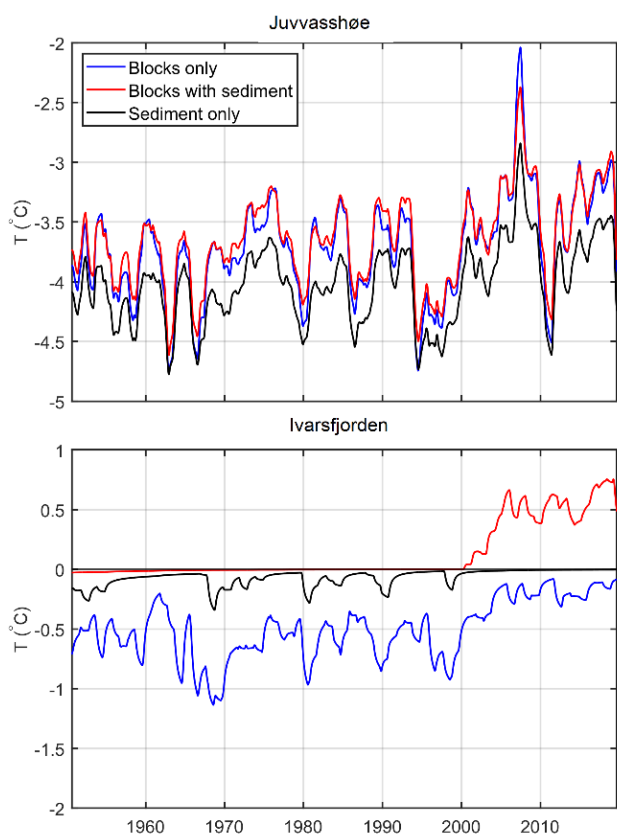
401 The ERA5 reanalysis dataset allows us to simulate the evolution of the ground thermal regime and ground ice content from
402 1951 to 2019, during which mean air temperatures increased from -4.5 °C (1951-1960) to -3.8 °C (2010-2019) for Juvvasshøe
403 and from 0.5 °C (1951-1960) to 1.2 °C (2010-2019) at Ivarsfjorden. **Fig. 7** shows the ground ice content for different scenarios
404 in Ivarsfjorden. In all simulations, a stable ice table and permafrost conditions form during the spin up period (using model
405 forcing for the cold period 1962-1971, Table 2), with volumetric ice contents of 0.5 (*blocks only, sediment only*) and of 0.25
406 (*blocks with sediment*) according to the applied stratigraphy (Table 1). In the period 1951 to 2019, ground ice content evolve
407 as a response to the applied climate forcing, showing different responses of the ground ice table. In the *blocks only, drained*
408 scenario, the perennial ice table in the upper 5 m (so between the active layer and the bedrock) does not lower by a significant
409 amount (2-% lowering), while the ice table lowers by 33 % in the *blocks only, undrained* scenario. The ice table in the *blocks*
410 *with sediment* stratigraphy disappears by 1985 and 1975 in the *undrained* and *drained* scenarios, respectively. Finally, the
411 *sediment only* simulations show an intermediate effect where the ice table has lowered by 41 % and 39 % for *undrained* and
412 *drained* conditions respectively by 2019. The complete degradation in the *blocks with sediment* runs compared to partial

413 degradation in all other scenarios (except *blocks only, drained*) is not unexpected since this stratigraphy has a 25% porosity
 414 (and thus ice content), compared to 50% in the others. We conclude that the ground stratigraphy and drainage conditions
 415 strongly control the response of the ground towards warming, with full degradation near-surface permafrost in both *blocks*
 416 *with sediment* runs, partial degradation in the *blocks only, undrained* run and in both *sediment only* runs and finally continued
 417 stable permafrost conditions in the *blocks only, drained* simulation. At the Juvvasshøe site, the ice table remain stable in all
 418 simulations, but a slight lowering occurs in the *blocks with sediment* scenarios.



419
 420 **Figure 8: Modelled volumetric ground ice content at Ivarsfjorden between 1951 and 2019 for the idealized stratigraphies in**
 421 ***undrained* and *drained* conditions and $sf = 1.0$. The ground surface elevation is at 106 m.a.s.l. In the active layer, ice contents increase**
 422 **and decrease annually, corresponding to the active layer refreezing and thawing.**

423 **Fig. 8** shows the change in temperatures at 5 m depth for the *drained* scenarios, which at the Ivarsfjorden rock glacier (snowfall
424 factor 1.0) correspond to a full (*blocks with sediment*) and partial (*sediment only*) lowering of the ice table, as well as a relatively
425 stable (*blocks only*) ice table. The *blocks only* simulation shows an increase from $-0.6\text{ }^{\circ}\text{C}$ to $-0.2\text{ }^{\circ}\text{C}$ between the 1951–1960
426 and 2010–2019 means, not being strongly influenced by latent heat effects due to the relative stable ice table. The *sediment*
427 *only* case experiences only minimal warming, as it is strongly influenced by the ongoing ground ice melt which confines
428 ground temperatures to close to $0\text{ }^{\circ}\text{C}$. Finally, the complete disappearance of ground ice in *blocks with sediment* run coincided
429 with in a warming to positive temperatures, from $0.0\text{ }^{\circ}\text{C}$ to $0.6\text{ }^{\circ}\text{C}$. At Juvvasshøe, permafrost degradation and thus strong
430 ground ice melt does not occur for any of the scenarios for snowfall factor 0.25, and ground temperatures only increased by
431 $0.2\text{ }^{\circ}\text{C}$ (*blocks only*) to $0.4\text{ }^{\circ}\text{C}$ (*blocks with sediment* and *sediment only*) between the 1951–1960 and 2010–2019 means (Fig.
432 8). The results of the transient runs indicate that the subsurface stratigraphy and drainage conditions strongly affect the timing
433 of permafrost degradation in blocky terrain. While ground ice melt controls the warming rates at Ivarsfjorden, only small
434 differences in warming rates are simulated for the still stable permafrost in Juvvasshøe. However, we emphasize that the
435 simulations at Juvvasshøe were performed for a shallow snow cover ($sf = 0.25$) for which differences in modeled ground
436 temperatures are small (Fig. 5).



437

438 **Figure 9:** Ground temperature at 5 m depth for the idealized stratigraphies under *drained* conditions; $sf = 1.0$ for Ivarsfjorden and
439 $sf = 0.25$ for Juvvasshøe.

440 5. Discussion

441 5.1 Limitations of the model setup

442 In this study, CryoGrid has been applied at two permafrost sites in Norwegian mountain environments. At both sites, we set
443 up validation runs to benchmark the performance of model system against measurements of ground (Juvvasshøe) and ground
444 surface (Ivarsfjorden) temperatures. At Juvvasshøe, the model can largely reproduce the annual cycle of measured ground
445 temperatures at the PACE borehole, when the snowfall is reduced to account for the generally shallow snow cover at the site.
446 At Ivarsfjorden, simulations with full snowfall yielded a similar performance for the ground surface temperature,
447 approximately reproducing the mean of measurements at 11 sites. A statistical evaluation at both sites indicated a cold bias of
448 the model of approximately -0.5 °C which we considered acceptable, considering the spatial variability of the ground thermal
449 regime at both sites (see Gislås et al. 2014 for Juvvasshøe). At Ivarsfjorden, the transient simulations are in broad agreement
450 with observations at the rock glacier which indicate that permafrost has been present in the recent past (Lilleøren et al., 2022).
451 Permafrost conditions are simulated for all stratigraphies during model spin using the cold period 1962-1971 for which
452 temperatures are closest to Little Ice Age conditions when the rock glacier was likely active.

453 Within the model setup, in particular the exact ground stratigraphy and other poorly constrained parameters, such as
454 the albedo, give rise to uncertainties. While the real porosity of the ground is unknown, sensitivity tests show a maximum of
455 0.4 °C differences in simulated ground temperatures between the highest and lowest porosity values tested (Supplement). Only
456 at Juvvasshøe, the stratigraphy has been described from the borehole (Isaksen et al., 2003), while no thorough evaluation of
457 the subsurface stratigraphy is available for Ivarsfjorden. Lilleøren et al. (2022) described the site as a complex creeping system
458 with inhomogeneous subsurface properties. Most of the rock glacier surface is described as ‘relict’ (Lilleøren et al., 2022) with
459 sand and gravel in between blocks. For these ‘relict’ areas, the simulations for the *blocks with sediment* stratigraphy, in which
460 near-surface permafrost fully or partially degrades, could indeed represent the thermal state adequately. This is supported by
461 the validation run with the *blocks with sediment* stratigraphy which yielded a good fit with ground surface temperature
462 measurements at sites largely located on this ‘relict’ surface (Lilleøren et al., 2022). Two areas are described as ‘fresh’ which
463 could indicate lateral movements due to the presence of ground ice. These contain larger blocks and could thus be better
464 described by the *blocks only* stratigraphy for which permafrost and ground ice still persist at the end of the simulations.
465 However, also in these ‘fresh’ areas, the amount of finer sediment is unclear, in particular in deeper layers. In our simulations,
466 we have only considered a single, homogeneous layer in the uppermost 5 m in order to compare the thermal regime and ground
467 ice dynamics for idealized stratigraphies. In reality, ground stratigraphies in blocky terrain can feature aspects of all scenarios,
468 for example a blocky layer with air-filled voids on top, followed by blocks filled with sediments and a sediment only layer in
469 the bottom. For the cooling effect described in this study, it is critical that the blocky top layer is deep enough so that a ground

470 ice table from which water can drain can form within. Therefore, it is likely that also shallower blocky layers with air-filled
471 voids can lead to lower ground temperatures, depending on the climatic conditions which determine the depth of the ground
472 ice table.

473 We emphasize that a consistent model setup was selected for all scenarios, so that uncertainties caused by other parts
474 of the model system influence them all in a similar, consistent way. In particular, none of the convective processes summarized
475 by Harris and Pedersen (1998) that cause a negative thermal anomaly in blocky terrain are considered in the model setup. The
476 same applies to the effect of rocks protruding into and through the snow cover as was described by Juliussen and Humlum
477 (2008) which could potentially be included in CryoGrid by laterally coupled simulations (e.g. Zweigel et al. 2021) with snow
478 redistribution between tiles representing blocks of different heights. Considering air convection in future simulations (as e.g.
479 in Wicky and Hauck, 2017) should become a priority for model development as this is likely to interact with the ground ice
480 mass balance for the blocky drained scenario and could thus exacerbate the thermal anomaly.

481 Further uncertainties are related to the model forcing data. The ERA5 reanalysis data is a global product with coarse
482 horizontal resolution, so that the TopoSCALE downscaling routine (Fiddes and Gruber 2014) is applied to obtain more
483 representative meteorological forcing. Nonetheless, as mentioned in Fiddes and Gruber (2014) and Fiddes et al. (2019; 2022),
484 there are limitations to this scheme, in particular the primitive downscaling scheme for precipitation, which only interpolates
485 between ERA5 grid points and thus misses the effects of local orography. The same is true for the effects of local cloud build-
486 up around slopes and mountains, which affects the radiation budget. While these uncertainties could affect the comparison of
487 model results to field measurements (Sect. 4.1), the model forcing data can certainly capture the regional-scale climate
488 characteristics of the two study sites, e.g. the significant differences in MAAT between the two sites. The thermal anomaly of
489 the *blocks only, drained* scenario consistently occurs for both sites and thus over a significant range of climate conditions, so
490 that the effect is likely robust despite the uncertainties in the model forcing data. The same is true for the uncertainty caused
491 by the Crocus-based snow scheme (Vionnet et al. 2012; Zweigel et al., 2021). In this study, we have performed a sensitivity
492 study with respect to the amount of snow (by modifying the snowfall factor, Sect. 4.2), but simply scaling snowfall cannot
493 represent the true time evolution of the snow cover due to wind redistribution (e.g. Liston & Sturm, 1998; Martin et al., 2019),
494 possibly resulting in differences between observed and simulated temperatures. Nevertheless, it seems unlikely that the exact
495 time dynamics of snow ablation and/or deposition events strongly affects the dependence of the thermal anomaly in the *blocks*
496 *only, drained* scenario on overall winter snow depths. We therefore conclude that the significant negative thermal anomaly for
497 the *blocks only, drained* scenario is likely robust in the light of the model uncertainty.

498 **5.2 The effect of the ground ice dynamics on ground temperatures**

499 Despite the uncertainties of the model setup, our results show a clear negative thermal anomaly for the *blocks only, drained*
500 scenario. If the winter snow depth is sufficiently high, a surface cover of coarse blocks with air-filled voids (i.e. high porosity
501 and low water holding capacity) results in 2 m ground temperatures 1 to 2 °C lower than for the other stratigraphies. In the
502 Ivarsfjorden simulations, the *blocks only, drained* scenario is the only one where near-surface permafrost conditions persist

503 even today, while near-surface permafrost degrades for the *blocks with sediment* and *sediment only* scenarios. This is
504 accompanied by a strong thermal offset, with a mean ground surface temperature of more than 2 °C for the *blocks only, drained*
505 scenario, while the mean ground temperatures at 2 m were below 0 °C. Interestingly, the temperature anomaly appears largely
506 constant over time in the transient simulations, except for periods when permafrost disappears in one of the scenarios and
507 confines ground temperatures to 0 °C, which delays further ground warming. For lower snow depths, the temperature anomaly
508 becomes smaller and eventually vanishes for the (largely irrelevant) case of permanently snow-free conditions.

509 The negative temperature anomaly largely accumulates during fall and winter (Fig. 6). The active layer contains very
510 little water in the *blocks only, drained* scenario. Dry soils have a lower thermal conductivity compared to wet soils, but the
511 lack of latent heat release allows for rapid refreezing during fall which enables fast cooling of the deeper soil layers and thus
512 leads to overall lower winter temperatures. In spring, this “cold content” (i.e. sensible heat) of the ground is partly transformed
513 into the build-up of new ground ice (i.e. latent heat, Fig. 7) which only melts slowly during summer due to the insulation of
514 the overlying blocky layer. This timing of the ground ice formation is strongly different from all other scenarios, for which
515 ground ice mostly forms in fall/early winter due to refreezing of the water contained in the active layer (e.g. Hinkel et al.,
516 2001). A somewhat similar effect has been described for peat plateaus in northern Norway where simulations yielded 2 °C
517 lower temperatures for well-drained peat compared to water-saturated peat (Martin et al., 2019). This refreezing of the active
518 layer can take several months and is further delayed if a significant snow cover forms during this period, which leads to overall
519 higher winter temperatures in the permafrost due to the insulation (Zhang, 2005). It is exactly for these “high-snow situations”
520 (corresponding to higher snowfall factors in our sensitivity analyses) that the temperature anomaly of the *blocks only, drained*
521 scenario is largest. Our results for example suggest that permafrost can occur for blocky ground on slopes around Juvvasshøe,
522 even if the winter snow cover exceeds 2 m thickness.

523 We note that the thermal anomaly caused by the ground ice dynamics in blocky ground is not related to convective
524 processes (Harris and Pedersen, 1998) or the effect of blocks protruding through the snow cover (Juliussen and Humlum, 2008;
525 Gruber Hoelzle, 2008). The simulated temperature anomaly is similar to the 1.3–2.0 °C lower temperatures that Juliussen and
526 Humlum (2008) found in blockfields compared to till and bedrock in Central-eastern Norway. While a complete process model
527 for blocky ground and rock glaciers will certainly have to take air convection and the interplay between surface blocks and the
528 snow cover into account, it is encouraging that the relatively simple model approach presented in this work offers prospects to
529 improve our estimates of permafrost occurrence in mountain environments.

530 In a first-order approach, thermal anomalies can be translated into elevation differences by assuming a temperature
531 lapse rate, so that the impacts on the lower altitudinal limit of permafrost can be estimated. For a lapse rate of 0.5 °C per 100
532 m (e.g. Farbrot et al., 2011), the lower limit of permafrost in drained, blocky deposits in Norway would be 300 to 400 m lower
533 compared to “normal” permafrost represented by the other scenarios. For the Ivarsfjorden site, these numbers compare
534 favorably to the Scandinavian permafrost map (Gisnås et al., 2017) which shows a lower discontinuous permafrost limit in
535 Finnmark at around 400 m a.s.l., approximately 300 m above the rock glacier.

536 5.3 Implications for future work

537 In this study, we show that modelling the full subsurface water and ice balance in well-drained blocky deposits with air-filled
538 voids leads to significantly lower ground temperatures in permafrost environments. In modelling studies on the distribution of
539 permafrost, blocky ground usually is not accounted for, or the water balance is not simulated at this level of detail. For the
540 Northern hemisphere permafrost map (Obu et al., 2019), a coarse landcover classification was used in mountain areas which
541 did not represent blocky terrain. To produce the map, a semi-empirical equilibrium TTOP model was used in which the thermal
542 anomaly of blocky deposits likely could account for by adjusting the r_k parameter which accounts for the thermal offset of the
543 ground. A more sophisticated modelling approach as presented in this work could be used to train the more simple TTOP
544 model across a range of climate conditions. Permafrost mapping with transient models (e.g. Jafarov et al., 2012) often uses
545 fixed ground stratigraphies, in which the sum of water and ice contents does not change for a given layer. An example is the
546 transient permafrost map for southern Norway (Westermann et al., 2013) which featured a dedicated stratigraphic class for
547 blocky deposits, with a dry upper layer followed by an ice-saturated layer below, very similar to the stratigraphy used for the
548 *blocks only, drained* scenario in this study. However, both layers have a fixed thickness and the sum of water and ice contents
549 is constant, so that the temporal evolution of ground ice dynamics cannot be captured. If the seasonal thaw extends in the ice-
550 rich layer, a pool of meltwater forms which cannot drain and hence strongly delays refreezing in fall, potentially resulting in
551 the degradation of permafrost. In our simulations with full water/ice dynamics, the ice table instead varies over time, both
552 seasonally and over longer periods in response to the climatic forcing. Such changes in the ground ice table have for example
553 been observed at the Schilthorn site in the European Alps where the ground ice table was significantly lowered during a hot
554 summer and did not regrow in the following years although permafrost conditions persisted (Hilbich et al., 2008). As this
555 observation site is located on a slope, it is clear that such observed ground ice dynamics can only be reproduced if lateral
556 drainage of meltwater is taken into account. To improve transient modelling of mountain permafrost distribution, CryoGrid in
557 the configuration used in this study could be adapted for individual grid cells, especially by adjusting the strength of the lateral
558 drainage (i.e. the distance to seepage face) depending on the local slope. In flat areas and depressions, water would then pool
559 up as for the *undrained* cases, while both melt- and rainwater would drain in sloping terrain as in the *undrained* cases, with
560 corresponding changes to the ground thermal regime and permafrost distribution. Furthermore, our study suggests that the
561 presence of fine sediments in the voids between blocks can strongly alter the ground temperature compared to blocky terrain
562 with air-filled voids. For spatially distributed mapping, these two cases would have to be distinguished as separate stratigraphic
563 classes and maps of their spatial extent must be available. Especially the latter is expected to be significant challenge, as the
564 surfaces likely appear similar for remote sensors, so that detailed field mapping may be required.

565 The model approach in this study also offers significant potential to study ground ice derived runoff from blocky
566 deposits and rock glaciers. While the Norwegian study sites are both located in wet climate settings with ample water supply,
567 rock glaciers in more arid regions can be important sources of water (e.g. Croce and Milana 2002). The global ratio of rock
568 glacier to glacier water volume equivalent (~~WVEQ~~) is currently increasing as both systems react differently to a changing

569 climate (Jones et al., 2019). Therefore, simulations of ground ice volumes and seasonal runoff characteristics in both the present
570 and future climates can be a valuable tool for the assessment of water resources. Furthermore, rock glaciers are sensitive to
571 climate change (Haeberli et al., 2010) and recent studies have linked rock glacier acceleration to increasing air temperatures
572 (e.g. Käab et al., 2007; Hartl et al., 2016; Eriksen et al., 2018). Our model approach is likely able to simulate the seasonal
573 ground ice mass balance at different points and elevations of a rock glacier which could be ingested in a flow model for rock
574 glaciers (e.g. Monnier and Kinnard, 2016). Finally, permafrost degradation and ground ice loss can also play an important role
575 for slope stability in mountain permafrost environments (e.g. Gruber and Haeberli, 2007; Saemundsson et al. 2018; Nelson et
576 al., 2001). Simulations of ground ice table changes, as well as the occurrence of strong melt events with corresponding
577 production of meltwater, could eventually improve assessments of the stability and hazard potential of permafrost-underlain
578 slopes (e.g. Mamot et al., 2021).

579 **6. Conclusions**

580 In this study, we used the CryoGrid permafrost model to simulate the effect of blocky terrain on the ground thermal regime
581 and ground ice dynamics at two Norwegian mountain permafrost sites (Juvvasshøe and Ivarsfjorden rock glacier). In particular,
582 we investigated the effect of subsurface drainage, as typical on slopes, for three idealized stratigraphies, named *blocks only*,
583 *blocks with sediment* and *sediment only*. From this study, the following conclusions can be drawn:

584

- 585 • Markedly lower ground temperatures are found in well drained, coarse blocky deposits with air-filled voids (*blocks*
586 *only, drained* scenario) compared to other scenarios which are either undrained or feature fine sediments. This
587 negative thermal anomaly can exceed 2 °C and is mainly linked to differences in the freeze-thaw dynamics caused
588 by the removal of meltwater and the build-up of new ground ice in spring. The largest anomalies occur in simulations
589 with a thick winter snow cover as ground temperatures in well drained blocky deposits are less sensitive to insulation
590 by snow than other soils. We emphasize that the model does not account for well-known factors, such as air
591 convection and the effect of blocks protruding through the winter snow cover.
- 592 • For the *blocks only, drained* scenario, thermally stable permafrost can exist at the Ivarsfjorden rock glacier site
593 (located near sea level), even for a mean annual ground surface temperature (~~MAGST~~) of 2.0–2.5 °C. At Juvvasshøe
594 in the southern Norwegian mountains, permafrost is simulated even for a very thick winter snow cover in the *blocks*
595 *only, drained* scenario, while all other scenarios in this case feature permafrost-free conditions.
- 596 • Transient simulations since 1951 at the Ivarsfjorden rock glacier show a completely or partially degraded ground ice
597 table for all scenarios, except the *blocks only, drained* scenario. This result is explained by the overall lower ground
598 temperatures in this scenario, while the simulated warming rates are generally similar for all scenarios, except for
599 periods when strong ground ice melt occurs.

600

601 This study suggests that including subsurface water and ice dynamics can drive simulations of mountain permafrost dynamics
602 towards reality, which can for example improve estimates of the lower altitudinal limit of permafrost in blocky terrain. In
603 addition to permafrost distribution mapping, the presented model approach could be used to simulate the seasonal and multi-
604 annual evolution of the ground ice table, in addition to ground-ice derived runoff. It therefore represents a further step to a
605 better understanding and model representation of the permafrost processes in mountain environments.

606

607 *Code and data availability.* The CryoGrid source code and model setup files are available
608 <https://doi.org/10.5281/zenodo.6563651> (Renette, 2022). Field measurements at Juvvasshøe are from Etzelmüller et al. (2020).
609 Field measurements at Ivarsfjorden are from Lilleøren et al. (2022).

610

611 *Author contribution.* CR performed the model simulations, retrieved forcing data, wrote the draft manuscript and created all
612 figures. SW helped design the study, developed the model and provided ideas throughout the entire study. KA developed code
613 for retrieving and downscaling forcing data, assisted with this process and wrote text regarding the forcing data. KL and KI
614 provided field measurements, site descriptions and photos. RBZ and JA developed parts of the model. All authors contributed
615 with text and suggestions.

616

617 *Competing interests.* The authors declare that they have no conflict of interest.

618

619 *Acknowledgements.* This work was supported by ESA Permafrost_CCI (<https://climate.esa.int/en/projects/permafrost/>),
620 Permafrost4Life (Research Council of Norway, grant no. 301639), and Nunataryuk (EU grant agreement no. 773421), as well
621 as the Department of Geosciences, University of Oslo.

622

623 **References**

- 624 Aalstad, K., Westermann, S., Schuler, T. V., Boike, J., and Bertino, L.: Ensemble-based assimilation of fractional snow-
625 covered area satellite retrievals to estimate the snow distribution at Arctic sites, *The Cryosphere*, 12, 247–270,
626 <https://doi.org/10.5194/tc-12-247-2018>, 2018.
- 627 Arenson, L. U., Phillips, M., and Springman, S. M.: Geotechnical considerations and technical solutions for infrastructure in
628 mountain permafrost, in: *New permafrost and glacier research*, pp. 3–50, Nova Science Publishers, 2009.
- 629 Azócar, G. and Brenning, A.: Hydrological and geomorphological significance of rock glaciers in the dry Andes, Chile (27–
630 33 S), *Permafrost and Periglacial Processes*, 21, 42–53, <https://doi.org/10.1002/ppp.669>, 2010.
- 631 Croce, F. A. and Milana, J. P.: Internal structure and behaviour of a rock glacier in the arid Andes of Argentina, *Permafrost
632 and Periglacial Processes*, 13, 289–299, <https://doi.org/10.1002/ppp.431>, 2002.
- 633 Dahl, R.: Block fields, weathering pits and tor-like forms in the Narvik Mountains, Nordland, Norway, *Geografiska Annaler:
634 Series A, Physical Geography*, 48, 55–85, <https://doi.org/10.1080/04353676.1966.11879730>, 1966.
- 635 Eriksen, H., Rouyet, L., Lauknes, T., Berthling, I., Isaksen, K., Hindberg, H., Larsen, Y., and Corner, G.: Recent acceleration
636 of a rock glacier complex, Adjet, Norway, documented by 62 years of remote sensing observations, *Geophysical Research
637 Letters*, 45, 8314–8323, <https://doi.org/10.1029/2018GL077605>, 2018.
- 638 Etzelmüller, B., Berthling, I., and Sollid, J. L.: Aspects and concepts on the geomorphological significance of Holocene
639 permafrost in southern Norway, *Geomorphology*, 52, 87–104, [https://doi.org/10.1016/S0169-555X\(02\)00250-7](https://doi.org/10.1016/S0169-555X(02)00250-7), 2003.
- 640 Etzelmüller, B., Schuler, T. V., Isaksen, K., Christiansen, H. H., Farbrot, H., and Benestad, R.: Modeling the temperature
641 evolution of Svalbard permafrost during the 20th and 21st century, *The Cryosphere*, 5, 67–79, [https://doi.org/10.5194/tc-5-67-
2011](https://doi.org/10.5194/tc-5-67-
642 2011), 2011.
- 643 Etzelmüller, B., Guglielmin, M., Hauck, C., Hilbich, C., Hoelzle, M., Isaksen, K., Noetzli, J., Oliva, M., and Ramos, M.:
644 Twenty years of European mountain permafrost dynamics—the PACE legacy, *Environmental Research Letters*, 15, 104070,
645 <https://doi.org/10.1088/1748-9326/abae9d>, 2020.
- 646 Farbrot, H., Hipp, T. F., Etzelmüller, B., Isaksen, K., Ødegård, R. S., Schuler, T. V., and Humlum, O.: Air and ground
647 temperature variations observed along elevation and continentality gradients in Southern Norway, *Permafrost and Periglacial
648 Processes*, 22, 343–360, <https://doi.org/10.1002/ppp.733>, 2011.
- 649 Fiddes, J. and Gruber, S.: TopoSCALE v. 1.0: downscaling gridded climate data in complex terrain, *Geoscientific Model
650 Development*, 7, 387–405, <https://doi.org/10.5194/gmd-7-387-2014>, 2014.
- 651 Fiddes, J., Endrizzi, S., and Gruber, S.: Large-area land surface simulations in heterogeneous terrain driven by global data sets:
652 application to mountain permafrost, *The Cryosphere*, 9, 411–426, <https://doi.org/10.5194/tc-9-411-2015>, 2015.
- 653 Fiddes, J., Aalstad, K., and Westermann, S.: Hyper-resolution ensemble-based snow reanalysis in mountain regions using
654 clustering, *Hydrology and Earth System Sciences*, 23, 4717–4736, <https://doi.org/10.5194/hess-23-4717-2019>, 2019.

655 Fiddes, J., Aalstad, K., and Lehning, M.: TopoCLIM: rapid topography-based downscaling of regional climate model output
656 in complex terrain v1. 1, *Geoscientific Model Development*, 15, 1753–1768, <https://doi.org/10.5194/gmd-15-1753-2022>,
657 2022.

658 Gislén, K., Eitzinger, B., Lussana, C., Hjørt, J., Sannel, A. B. K., Isaksen, K., Westermann, S., Kuhry, P., Christiansen, H.
659 H., Frampton, A., et al.: Permafrost map for Norway, Sweden and Finland, *Permafrost and periglacial processes*, 28, 359–378,
660 <https://doi.org/10.1002/ppp.1922>, 2017.

661 Gislén, K., S. Westermann, T. V. Schuler, T. Litherland, K. Isaksen, J. Boike, and B. Eitzinger.: A statistical approach to
662 represent small-scale variability of permafrost temperatures due to snow cover, *The Cryosphere*, 8.6, pp. 2063–2074.
663 <https://doi.org/10.5194/tc-8-2063-2014>, 2014.

664 Gislén, K., Westermann, S., Schuler, T. V., Melvold, K., and Eitzinger, B.: Small-scale variation of snow in a regional
665 permafrost model, *The Cryosphere*, 10, 1201–1215, <https://doi.org/10.5194/tc-10-1201-2016>, 2016.

666 Göckede, M., Kittler, F., Kwon, M. J., Burjack, I., Heimann, M., Kolle, O., et al.: Shifted energy fluxes, increased Bowen
667 ratios, and reduced thaw depths linked with drainage-induced changes in permafrost ecosystem structure, *The Cryosphere*,
668 11(6), 2975–2996. <https://doi.org/10.5194/tc-11-2975-2017>, 2017.

669 Goodrich, L. E.: The influence of snow cover on the ground thermal regime, *Can. Geotech. J.*, 19, 421–432,
670 <https://doi.org/10.1139/t82-047>, 1982.

671 Gruber, S. and Haeberli, W.: Permafrost in steep bedrock slopes and its temperature-related destabilization following climate
672 change, *Journal of Geophysical Research: Earth Surface*, 112, <https://doi.org/10.1029/2006JF000547>, 2007.

673 Gruber, S. and Hoelze, M.: The cooling effect of coarse blocks revisited: a modeling study of a purely conductive mechanism,
674 *Zurich Open Repository and Archive*, 2008.

675 Haeberli, W., Hallet, B., Arenson, L., Elconin, R., Humlum, O., Käab, A., Kaufmann, V., Ladanyi, B., Matsuoka, N.,
676 Springman, S., et al.: Permafrost creep and rock glacier dynamics, *Permafrost and periglacial processes*, 17, 189–214,
677 <https://doi.org/10.1002/ppp.561>, 2006.

678 Hanson, S. and Hoelzle, M.: The thermal regime of the active layer at the Murtèl rock glacier based on data from 2002,
679 *Permafrost and Periglacial Processes*, 15, 273–282, <https://doi.org/10.1002/ppp.499>, 2004.

680 Harris, C., Haeberli, W., Vonder Mühl, D., and King, L.: Permafrost monitoring in the high mountains of Europe: the PACE
681 project in its global context, *Permafrost and periglacial processes*, 12, 3–11, <https://doi.org/10.1002/ppp.377>, 2001.

682 Harris, C., Arenson, L. U., Christiansen, H. H., Eitzinger, B., Frauenfelder, R., Gruber, S., Haeberli, W., Hauck, C., Hoelzle,
683 M., Humlum, O., et al.: Permafrost and climate in Europe: Monitoring and modelling thermal, geomorphological and
684 geotechnical responses, *EarthScience Reviews*, 92, 117–171, <https://doi.org/10.1016/j.earscirev.2008.12.002>, 2009.

685 Harris, S. A. and Pedersen, D. E.: Thermal regimes beneath coarse blocky materials, *Permafrost and periglacial processes*, 9,
686 107–120, [https://doi.org/10.1002/\(SICI\)1099-1530\(199804/06\)9:2<107::AID-PPP277>3.0.CO;2-G](https://doi.org/10.1002/(SICI)1099-1530(199804/06)9:2<107::AID-PPP277>3.0.CO;2-G), 1998.

687 Hartl, L., Fischer, A., Stocker-waldhuber, M., and Abermann, J.: Recent speed-up of an alpine rock glacier: an updated
688 chronology of the kinematics of outer hochebenkar rock glacier based on geodetic measurements, *Geografiska Annaler: Series*
689 *A, Physical Geography*, 98, 129–141, <https://doi.org/10.1111/geoa.12127>, 2016.

690 Hersbach, H., Bell, B., Berrisford, P., Hirahara, S., Horányi, A., Muñoz-Sabater, J., Nicolas, J., Peubey, C., Radu, R., Schepers,
691 D., et al.: The ERA5 global reanalysis, *Quarterly Journal of the Royal Meteorological Society*, 146, 1999–2049,
692 <https://doi.org/10.1002/qj.3803>, 2020.

693 Hilbich, C., Hauck, C., Hoelzle, M., Scherler, M., Schudel, L., Völksch, I., Vonder Mühll, D., and Mäusbacher, R.: Monitoring
694 mountain permafrost evolution using electrical resistivity tomography: A 7-year study of seasonal, annual, and long-term
695 variations at Schilthorn, Swiss Alps, *Journal of Geophysical Research: Earth Surface*, 113,
696 <https://doi.org/10.1029/2007JF000799>, 2008.

697 Hinkel, K. M. and Outcalt, S. I.: Identification of heat transfer processes during soil cooling, freezing, and thaw in central
698 Alaska, *Permafrost Periglac.*, 5, 217–235, <https://doi.org/10.1002/ppp.3430050403>, 1994.

699 Hinkel, K. M., Paetzold, F., Nelson, F. E., and Bockheim, J. G.: Patterns of soil temperature and moisture in the active layer
700 and upper permafrost at Barrow, Alaska: 1993–1999, *Global Planet. Change*, 29, 293–309, 2001.

701 Hipp, T., Etzelmüller, B., Farbrot, H., Schuler, T., and Westermann, S.: Modelling borehole temperatures in Southern Norway–
702 insights into permafrost dynamics during the 20th and 21st century, *The Cryosphere*, 6, 553–571, [https://doi.org/10.5194/tc-](https://doi.org/10.5194/tc-6-553-2012)
703 [6-553-2012](https://doi.org/10.5194/tc-6-553-2012), 2012.

704 Humlum, O.: Active layer thermal regime at three rock glaciers in Greenland, *Permafrost and Periglacial Processes*, 8, 383–
705 408, [https://doi.org/10.1002/\(SICI\)1099-1530\(199710/12\)8:4<383::AID-PPP265>3.0.CO;2-V](https://doi.org/10.1002/(SICI)1099-1530(199710/12)8:4<383::AID-PPP265>3.0.CO;2-V), 1997.

706 Isaksen, K., Holmlund, P., Sollid, J. L., and Harris, C.: Three deep alpine-permafrost boreholes in Svalbard and Scandinavia,
707 *Permafrost and Periglacial Processes*, 12, 13–25, <https://doi.org/10.1002/ppp.380>, 2001.

708 Isaksen, K., Heggem, E., Bakkehøi, S., Ødegård, R., Eiken, T., Etzelmüller, B., and Sollid, J.: Mountain permafrost and energy
709 balance on Juvvasshøe, southern Norway, in: 8th International Conference on Permafrost, Zurich, Switzerland, ISI:
710 000185049300083, pp. 467–472, 2003.

711 Isaksen, K., Sollid, J. L., Holmlund, P., and Harris, C.: Recent warming of mountain permafrost in Svalbard and Scandinavia,
712 *Journal of Geophysical Research: Earth Surface*, 112, <https://doi.org/10.1029/2006JF000522>, 2007.

713 Jafarov, E. E., Marchenko, S. S., and Romanovsky, V.: Numerical modeling of permafrost dynamics in Alaska using a high
714 spatial resolution dataset, *The Cryosphere*, 6, 613–624, <https://doi.org/10.5194/tc-6-613-2012>, 2012.

715 Jones, D. B., Harrison, S., Anderson, K., and Whalley, W. B.: Rock glaciers and mountain hydrology: A review, *Earth-Science*
716 *Reviews*, 193, 66–90, <https://doi.org/10.1016/j.earscirev.2019.04.001>, 2019.

717 Juliussen, H. and Humlum, O.: Thermal regime of openwork block fields on the mountains Elgåhogna and Sølen, central-
718 eastern Norway, *Permafrost and Periglacial Processes*, 19, 1–18, <https://doi.org/10.1002/ppp.607>, 2008.

719 Kääb, A., Frauenfelder, R., and Roer, I.: On the response of rockglacier creep to surface temperature increase, *Global and*
720 *Planetary Change*, 56, 172–187, <https://doi.org/10.1016/j.gloplacha.2006.07.005>, 2007.

721 Langer, M., Westermann, S., Boike, J., Kirillin, G., Grosse, G., Peng, S., and Krinner, G.: Rapid degradation of permafrost
722 underneath waterbodies in tundra landscapes—toward a representation of thermokarst in land surface models, *Journal of*
723 *Geophysical Research: Earth Surface*, 121, 2446–2470, <https://doi.org/10.1002/2016JF003956>, 2016.

724 Liestøl, O.: Lokalt omrøde med permafrost i Gudbrandsdalen, *Norsk Polarinstitutt Aarbok*, 1965, 129-133, 1966.

725 Liljedahl, A. K., Hinzman, L. D., Harazono, Y., Zona, D., Tweedie, C. E., Hollister, R. D., et al.: Nonlinear controls on
726 evapotranspiration in Arctic coastal wetlands. *Biogeosciences*, 8(11), 3375–3389. <https://doi.org/10.5194/bg-8-3375-2011>,
727 2011.

728 Lilleøren, K. S. and Eitzelmüller, B.: A regional inventory of rock glaciers and ice-cored moraines in Norway, *Geografiska*
729 *Annaler: Series A, Physical Geography*, 93, 175–191, <https://doi.org/10.1111/j.1468-0459.2011.00430.x>, 2011.

730 Lilleøren, K. S., Eitzelmüller, B., Rouyet, L., Eiken, T., and Hilbich, C.: Transitional rock glaciers at sea-level in Northern
731 Norway, *Earth Surface Dynamics Discussions*, pp. 1–29, <https://doi.org/10.5194/esurf-2022-6>, 2022.

732 Liston, G. E. and Sturm, M.: A snow-transport model for complex terrain, *Journal of Glaciology*, 44, 498–516,
733 <https://doi.org/10.3189/S0022143000002021>, 1998.

734 Luetsch, M., Stoeckli, V., Lehning, M., Haeblerli, W., and Ammann, W.: Temperatures in two boreholes at Flüela Pass,
735 Eastern Swiss Alps: the effect of snow redistribution on permafrost distribution patterns in high mountain areas, *Permafrost*
736 *Periglac.*, 15, 283–297, doi:10.1002/ppp.500, 2004.

737 Mamot, P., Weber, S., Eppinger, S., and Krautblatter, M.: A temperature-dependent mechanical model to assess the stability
738 of degrading permafrost rock slopes, *Earth Surface Dynamics*, 9, 1125–1151, <https://doi.org/10.5194/esurf-9-1125-2021>,
739 2021.

740 Martin, L. C. P., Nitzbon, J., Aas, K. S., Eitzelmüller, B., Kristiansen, H., and Westermann, S.: Stability conditions of peat
741 plateaus and palsas in northern Norway, *Journal of Geophysical Research: Earth Surface*, 124, 705–719,
742 <https://doi.org/10.1029/2018JF004945>, 2019.

743 Monnier, S. and Kinnard, C.: Interrogating the time and processes of development of the Las Liebres rock glacier, central
744 Chilean Andes, using a numerical flow model, *Earth Surface Processes and Landforms*, 41, 1884–1893,
745 <https://doi.org/10.1002/esp.3956>, 2016.

746 Nelson, F. E., Anisimov, O. A., and Shiklomanov, N. I.: Subsidence risk from thawing permafrost, *Nature*, 410, 889–890,
747 <https://doi.org/10.1038/35073746>, 2001.

748 Nesje, A., Matthews, J. A., Linge, H., Bredal, M., Wilson, P., and Winkler, S.: New evidence for active talus-foot rock glaciers
749 at Øyberget, southern Norway, and their development during the Holocene, *The Holocene*, 31, 1786–1796,
750 <https://doi.org/10.1177/09596836211033226>, 2021.

751 Obu, J., Westermann, S., Bartsch, A., Berdnikov, N., Christiansen, H. H., Dashtseren, A., Delaloye, R., Elberling, B.,
752 Eitzelmüller, B., Kholodov, A., et al.: Northern Hemisphere permafrost map based on TTOP modelling for 2000–2016 at 1
753 km² scale, *Earth-Science Reviews*, 193, 299–316, <https://doi.org/10.1016/j.earscirev.2019.04.023>, 2019.

754 Painter, S. L. and Karra, S.: Constitutive model for unfrozen water content in subfreezing unsaturated soils, *Vadose Zone*
755 *Journal*, 13, <https://doi.org/10.2136/vzj2013.04.0071>, 2014.

756 Porter, C., Morin, P., Howat, I., Noh, M., Bates, B., Peterman, K., Keeseey, S., Schlenk, M., Gardiner, J., Tomko, K., et al.:
757 ArcticDEM, Harvard Dataverse [data set], V1, <https://doi.org/10.7910/DVN/OHHUKH>, 2018.

758 Renette, C.: Parameter files and code for simulations in "Simulating the effect of subsurface drainage on the thermal regime
759 and ground ice in blocky terrain, Norway" [Data set], Zenodo, <https://doi.org/10.5281/zenodo.6563651>, 2022.

760 Romundset, A., Bondevik, S., and Bennike, O.: Postglacial uplift and relative sea level changes in Finnmark, northern Norway,
761 *Quat. Sci. Rev.*, 30, 2398-2421, <https://doi.org/10.1016/j.quascirev.2011.06.007>, 2011.

762 Sæmundsson, Þ., Morino, C., Helgason, J. K., Conway, S. J., and Pétursson, H. G.: The triggering factors of the Móafellshyrna
763 debris slide in northern Iceland: Intense precipitation, earthquake activity and thawing of mountain permafrost, *Science of the*
764 *total environment*, 621, 1163–1175, <https://doi.org/10.1016/j.scitotenv.2017.10.111>, 2018.

765 Saloranta, T.: Simulating snow maps for Norway: description and statistical evaluation of the seNorge snow model, *The*
766 *Cryosphere*, 6, 1323–1337, <https://doi.org/10.5194/tc-6-1323-2012>, 2012.

767 Scudeler, C., Paniconi, C., Pasetto, D., and Putti, M.: Examination of the seepage face boundary condition in subsurface and
768 coupled surface/subsurface hydrological models, *Water Resources Research*, 53(3), 1799-1819, 2017.

769 Schmidt, J. U., Etzelmüller, B., Schuler, T. V., Magnin, F., Boike, J., Langer, M., and Westermann, S.: Surface temperatures
770 and their influence on the permafrost thermal regime in high-Arctic rock walls on Svalbard, *The Cryosphere*, 15, 2491–2509,
771 <https://doi.org/10.5194/tc-15-2491-2021>, 2021.

772 Smith, M. and Riseborough, D.: Climate and the limits of permafrost: a zonal analysis, *Permafrost and Periglacial Processes*,
773 13, 1–15, <https://doi.org/10.1002/ppp.410>, 2002.

774 Van Everdingen, R. O.: Multi-language glossary of permafrost and related ground-ice terms, *International Permafrost*
775 *Association*, 1998.

776 Vionnet, V., Brun, E., Morin, S., Boone, A., Faroux, S., Le Moigne, P., Martin, E., and Willemet, J.-M.: The detailed snowpack
777 scheme Crocus and its implementation in SURFEX v7. 2, *Geoscientific Model Development*, 5, 773–791,
778 <https://doi.org/10.5194/gmd-5-773-2012>, 2012.

779 Westermann, S., Schuler, T., Gislås, K., and Etzelmüller, B.: Transient thermal modeling of permafrost conditions in Southern
780 Norway, *The Cryosphere*, 7, 719–739, <https://doi.org/10.5194/tc-7-719-2013>, 2013.

781 Westermann, S., Langer, M., Boike, J., Heikenfeld, M., Peter, M., Etzelmüller, B., and Krinner, G.: Simulating the thermal
782 regime and thaw processes of ice-rich permafrost ground with the land-surface model CryoGrid 3, *Geoscientific Model*
783 *Development*, 9, 523–546, <https://doi.org/10.5194/gmd-9-523-2016>, 2016.

784 Westermann, S., Ingeman-Nielsen, T., Scheer, J., Aalstad, K., Aga, J., Chaudhary, N., Etzelmüller, B., Filhol, S., Kääb, A.,
785 Renette, C., Schmidt, L. S., Schuler, T. V., Zweigel, R. B., Martin, L., Morard, S., Ben-Asher, M., Angelopoulos, M., Boike,
786 J., Groenke, B., Miesner, F., Nitzbon, J., Overduin, P., Stuenzi, S. M., and Langer, M.: The CryoGrid community model

787 (version 1.0) – a multi-physics toolbox for climate-driven simulations in the terrestrial cryosphere, *Geosci. Model Dev.*
788 *Discuss.* [preprint], <https://doi.org/10.5194/gmd-2022-127>, in review, 2022.

789 Wicky, J. and Hauck, C.: Numerical modelling of convective heat transport by air flow in permafrost talus slopes, *The*
790 *Cryosphere*, 11, 1311–1325, <https://doi.org/10.5194/tc-11-1311-2017>, 2017.

791 Zhang, T.: Influence of the seasonal snow cover on the ground thermal regime: An overview, *Reviews of Geophysics* 43.4,
792 <https://doi.org/10.1029/2004RG000157>, 2005.

793 Zweigel, R., Westermann, S., Nitzbon, J., Langer, M., Boike, J., Eitzelmüller, B., and Vikhamar Schuler, T.: Simulating snow
794 redistribution and its effect on ground surface temperature at a high-Arctic site on Svalbard, *Journal of Geophysical Research:*
795 *Earth Surface*, 126, e2020JF005673, <https://doi.org/10.1029/2020JF005673>, 2021.

796